OXFORD

Human Molecular Genetics, 2022, Vol. 31, 12, 1946–1961
https://doi.org/10.1093/hmg/ddab372
Advance access publication date 31 December 2021
Original Article

Systematic identification of genomic elements that regulate *FCGR2A* expression and harbor variants linked with autoimmune disease

Johanna Dahlqvist[1,6], Charles P. Fulco[1,2,7], John P. Ray[1,8], Thomas Liechti[3], Carl G. de Boer[4,9], David J. Lieb[1], Thomas M. Eisenhaure[1], Jesse M. Engreitz[1,10,11], Mario Roederer[3] and Nir Hacohen[1,5,*]

[1]Center for Cell Circuits, Broad Institute of MIT and Harvard University, Cambridge, MA 02142, USA
[2]Department of Systems Biology, Harvard Medical School, Boston, MA 02115, USA
[3]ImmunoTechnology Section, Vaccine Research Center, NIAID, NIH, Bethesda, MD 20814, USA
[4]Klarman Cell Observatory, Broad Institute of MIT and Harvard University, Cambridge, MA 02142, USA
[5]Center for Cancer Research, Massachusetts General Hospital, Boston, MA 02114, USA
[6]Present address: Department of Medical Sciences, Uppsala University, 751 85 Uppsala, Sweden
[7]Present address: Bristol Myers Squibb, Cambridge, MA 02142, USA
[8]Present address: Systems Immunology, Benaroya Research Institute, Seattle, WA 98101, USA
[9]School of Biomedical Engineering, University of British Columbia, Vancouver, BC V6T 1Z4, Canada
[10]Present address: Department of Genetics, Stanford University School of Medicine, Stanford, CA, USA
[11]Present address: BASE Initiative, Betty Irene Moore Children's Heart Center, Lucile Packard Children's Hospital, Stanford University School of Medicine, Stanford, CA, USA
*To whom correspondence should be addressed at: The Broad Institute of MIT and Harvard University, 415 Main Street, Cambridge, MA 02142, USA. Tel: +1 6177147234, Fax: +1 6177148956; Email: nhacohen@mgh.harvard.edu

Abstract

Background: FCGR2A binds antibody–antigen complexes to regulate the abundance of circulating and deposited complexes along with downstream immune and autoimmune responses. Although the abundance of FCRG2A may be critical in immune-mediated diseases, little is known about whether its surface expression is regulated through *cis* genomic elements and non-coding variants. In the current study, we aimed to characterize the regulation of FCGR2A expression, the impact of genetic variation and its association with autoimmune disease. *Methods:* We applied CRISPR-based interference and editing to scrutinize 1.7 Mb of open chromatin surrounding the *FCGR2A* gene to identify regulatory elements. Relevant transcription factors (TFs) binding to these regions were defined through public databases. Genetic variants affecting regulation were identified using luciferase reporter assays and were verified in a cohort of 1996 genotyped healthy individuals using flow cytometry. *Results:* We identified a complex proximal region and five distal enhancers regulating *FCGR2A*. The proximal region split into subregions upstream and downstream of the transcription start site, was enriched in binding of inflammation-regulated TFs, and harbored a variant associated with FCGR2A expression in primary myeloid cells. One distal enhancer region was occupied by CCCTC-binding factor (CTCF) whose binding site was disrupted by a rare genetic variant, altering gene expression. *Conclusions:* The *FCGR2A* gene is regulated by multiple proximal and distal genomic regions, with links to autoimmune disease. These findings may open up novel therapeutic avenues where fine-tuning of FCGR2A levels may constitute a part of treatment strategies for immune-mediated diseases.

Introduction

Immune complexes (ICs), composed of immunoglobulins and antigens, are critical factors in the physiological immune response against microbes, autoimmune diseases and antibody-based therapeutics (1–3). In humans, large ICs are cleared by the mononuclear phagocytic system, whereas moderate sized and small ICs that contain IgG bind to low-affinity Fc gamma receptors (FCGRs) and trigger immune responses via the activating receptors FCGR2A and FCGR3A. FCGR2A is expressed on granulocytes, monocytes, macrophages, dendritic cells (DCs), plasmacytoid DCs, platelets and endothelial cells (4). Upon IC binding, the receptor is cross-linked and phosphorylated by Srk and Syk family kinases, initiating an intracellular signaling cascade leading to cell activation and transcriptional induction of chemokines and cytokines, such as interleukin 1β (IL-1β) and tumor necrosis factor-α [TNF-α; (5)]. Moreover, cross-linking of FCGR2A leads to phagocytosis and degradation of ICs and subsequent cross-presentation of antigens on major histocompatibility complex molecules to CD4+ and CD8+ T cells (6). FCGR2A has been functionally implicated in cardiovascular, infectious and autoimmune diseases (7–10) and recently in the emerging field of antibody-based cancer treatments (11).

The *FCGR2A* locus has been genetically associated with both autoimmune and infectious diseases, such as systemic lupus erythematosus (SLE), ulcerative colitis,

Received: October 27, 2021. **Revised:** December 20, 2021. **Accepted:** December 23, 2021

Kawasaki's disease, pneumococcal infection and sepsis (7,8,12–14). The signal of association has been attributed to a missense variant in exon 4 (rs1801274, c.497A > G; NM_001375297.1), as the variant causes an amino acid switch (p.H166R) in the binding pocket of the receptor, reducing the affinity of the receptor for IgG2 (15). However, genetically, there is a relatively low posterior probability of the missense variant being the causal variant according to a genome-wide association study of SLE in Europeans (16); furthermore, a trans-ethnic study with fine mapping of the *FCGR2A* locus has implicated non-coding single-nucleotide polymorphisms (SNPs) as the source of association with SLE at this locus (17). In addition, rheumatoid arthritis (RA) has a suggestive association ($P < 1 \times 10^{-4}$) with two non-coding variants in tight linkage disequilibrium (LD) at the FCGR2A locus (18,19). Hence, the exact mechanism by which genetic variants at the *FCGR2A* locus facilitate an autoimmune state remains elusive.

The current understanding of how FCGR2A is regulated is poorly understood. It is well established that in the human genome, regulation of gene expression is dependent on the interaction between distal regulatory regions and the promoter region and, additionally, that the enhancer regions do not always affect expression of the closest gene but may act on more distant genes (20). Consequently, limited analysis of open chromatin or chromatin immunoprecipitation sequencing analysis (ChIP-Seq) of histone modifications marking regulatory regions cannot distinguish what regions act on what genes (21,22). Lately, several studies have successfully identified proximal and distal regulatory regions of selected genes, using clustered regularly interspaced short palindromic repeats (CRISPR) interference, a technology based on the CRISPR/Cas9 editing technique, but with an enzymatically inactive Cas9 (dCas9) fused to the heterochromatin-inducing Krüppel associated box (KRAB) domain (23–25). The dCas9-KRAB complex results in rapid histone deacetylation and tri-methylation at histone 3 leucine 9 (H3K9me3) at a region targeted by single-guide RNAs (sgRNAs), thus silencing regulatory regions that act as enhancers of promoters (25,26). Similarly, several studies have interrogated cis-regulatory regions using screens based on CRISPR/Cas9 cutting (27,28). However, although CRISPR interference (CRISPRi) is an efficient tool for identifying enhancer/promoter regions and CRISPR/Cas9 cutting may delineate limited regulatory elements, few studies have combined the use of CRISPRi and CRISPR/Cas9 cutting and taken advantage of their respective benefits in identifying and scrutinizing regulatory regions (29,30).

In this study, we hypothesized that specific genomic elements and genetic variants regulate the expression of FCGR2A and thus modulate immunity and impact immune-mediated diseases. We mapped the *cis* regions affecting expression of *FCGR2A* in detail using CRISPR/Cas9 and CRISPRi techniques and analyzed key TFs associated with these regulatory elements. We identified disease-associated genetic variants affecting gene expression as well as cell surface expression of the gene product. Collectively, our findings uncover novel regulatory regions that alter FCGR2A expression, and prioritize regulatory variants with a possible impact on susceptibility to disease.

Results

FCGR2A transcription is regulated by an extensive proximal region and five distal enhancers interspersed between FCGR genes

FCGR2A is of critical importance for clearance of ICs and activation of immune response (31), but little is known about the mechanisms behind the regulation of FCGR2A expression. We hypothesized that *FCGR2A* gene expression is regulated in response to differential concentrations of ICs. When primary monocytes were exposed to ICs *ex vivo*, *FCGR2A* mRNA expression increased (Supplementary Material, Fig. S1A), in line with increased transcript levels of *FCGR2A* detected in freshly isolated myeloid cells from patients with the IC-associated diseases sepsis and SLE [Supplementary Material, Fig. S1B and C; (32,33)]. To better understand the regulation of FCGR2A expression, we used CRISPRi to identify genetic regions that control *FCGR2A* transcript levels. To set the boundaries for the genomic region to be analyzed, we performed a chromosome conformation capture (4C) analysis with the *FCGR2A* transcription start site (TSS) as anchor in the myeloid leukemia cell line U937. Interacting genomic loci were identified within ~400 kb (kilo bases; chr1:161 400 000–161 800 000), consistent with the topologically associated domain (TAD) encompassing the FCGRs observed in Hi-C data in the K562 (erythroleukemia) and THP-1 (acute monocytic leukemia) cell lines [(34,35); Supplementary Material, Fig. S2]. To capture this TAD and more distant regions, we assessed the functions of putative *cis* regulatory regions in a 1.7 mega base (Mb) interval centered on *FCGR2A* (in total 5 TADs).

To systematically analyze the assigned region for regulatory effects on FCGR2A, we designed a lentiviral library of 22 471 sgRNAs targeting all regions of open chromatin within the defined TADs (Supplementary Material, Fig. S3). The library was transduced into resting monocytic U937 cells treated with doxycycline to upregulate a stably integrated doxycycline-inducible dCas9 fused to the transcriptional repressor KRAB. To find sgRNAs that affect FCGR2A levels, we stained cells using anti-FCGR2A antibody, flow-sorted cells into gates of the highest or lowest 10% FCGR2A expression and then sequenced sgRNAs (that were inserted into the genome) to determine their enrichment or depletion in each gate [see Materials and Methods and Supplementary Material, Table S1; (25)]. We identified six regulatory regions within the *FCGR2A* TAD (hereby referred to as 'regions 1–6'; Fig. 1A; Supplementary Material, Table S2), and one region located upstream of the FCGR2A TAD in the CD244 gene, (Supplementary Material, Fig. S4;

Supplementary Material, Table S2). Since the CD244 region does not physically interact with the FCGR2A promoter region according to K562 and THP-1 Hi-C data (Supplementary Material, Fig. S4), this region was not further pursued in the study. Instead we focused on the six regions within the *FCGR2A* TAD, located from 64 kilo bases (kb) upstream to 116 kb downstream from the *FCGR2A* TSS. The most 5′ distal region was confined to the boundary of the TAD, and the two most 3′ distal regions localized to the 3′ end of the *FCGR3A* and *FCGR3B* genes, respectively. FCGR2A expression is thus regulated by multiple genomic regions interspersed among FCGR and heat shock protein genes, in resting myeloid cells.

According to publicly available data in U937 cells and primary human CD14$^+$ monocytes, all six regions but region 2 were marked by the enhancer histone signature H3K27Ac (Fig. 1A). All regions but region 4 showed open chromatin (based on DNase/ATAC-seq accessibility assays) in a wide range of cell types (Supplementary Material, Fig. S5) and regions 1, 2, 5 and 6 exhibited increased interactions with the proximal regulatory region (region 3) based on K562 5 kb resolution- and THP-1 10 kb resolution Hi-C data (Fig. 1B; Supplementary Material, Fig. S3). The six regions overlapped TF chromatin ChIP-Seq hot spots in multiple cell types (Supplementary Material, Fig. S5); notably, regions 1 and 2 showed strong binding of CCCTC-binding factor (CTCF) in 97 out of 99 analyzed cell types (Fig. 1C). Enrichment analysis of the complete set of TFs with ChIP-Seq signals in regions 1–6 revealed an association with immune response-regulating cell surface receptor signaling pathway, positive regulation of type I IFN production, cytokine response and regulation of megakaryocyte, myeloid, endothelial and DC differentiation (Supplementary Material, Tables S3–S6). Together, the regulatory function of regions 1–6 in myeloid cells is further supported by existing epigenetic and topological data.

FCGR2A expression is directed by two proximal subregions encompassing elements with both activating and inhibitory effects and binding of inflammation-associated TFs

Based on the CRISPRi experiments described earlier, silencing of region 3 (an 8.8 kb region spanning from 7.2 kb 5′ of the TSS into intron 3) showed the largest effect on FCGR2A levels (Fig. 2A and B). Because dCas9-KRAB can induce silencing over a region of 100–1000 s of base pairs [bps; (25,26)], we conducted a second screen using enzymatically active Cas9 that cleaves DNA to achieve higher resolution. We tiled 1848 gRNAs across an extended region 3, including potentially regulatory sequences 5′ of *FCGR2A*, based on H3K4me1 and H3K27Ac modifications in K562 cells and CD14$^+$ monocytes. In addition to the expected reduction in FCGR2A expression at targeted exons, we found sgRNA-induced reduction in two subregions, overlapping the highest level of chromatin accessibility in U937 cells and CD14$^+$ monocytes. One Subregion 5′ of the TSS (Subregion 1, within region 3), had the strongest signal within 40 bps of the TSS but stretching up to ∼250 bps upstream. A second subregion (Subregion 2, within region 3) in intron 3, had strongly scoring sgRNAs at the 40 bps after the junction with exon 3. In addition, in Subregion 2, ∼225–290 bps from exon 3, strongly scoring sgRNAs increased FCGR2A expression [Figs 1 and 2A and B (gray boxes); Supplementary Material, Table S7]. Both subregions overlapped peaks of open chromatin in CD14$^+$ monocytes and TF peaks in myeloid cells (Fig. 2), and the sequences where sgRNAs reduced FCGR2A expression showed enhancing activities using luciferase reporters (Supplementary Material, Fig. S6), suggesting that these two subregions are critical for regulation of *FCGR2A* expression.

To identify TFs that bind at the first and second subregions described earlier in primary myeloid cells, we analyzed available data in the Chip-atlas database (36) for CD14$^+$ monocytes, macrophages, DCs as well as U937 cells. We identified three areas with TF binding. First, overlapping Subregion 1 (5′ of the TSS), STAT1 binding was found in resting and in IFN-γ or lipopolysaccharide (LPS)-stimulated CD14$^+$ monocytes; SPI1 and SREBF2 binding in macrophages and CEBPA and SMAD1 in U937 cells (Fig. 2A and B). Second, overlapping Subregion 2 (downstream of exon 3), binding of STAT1 and IRF1 in CD14$^+$ monocytes; ZNF366 in DCs; SPI1 (with and without IFN-γ), SREBF2 (with TNF- α), SMC1A (with IFN-γ), CEBPB in macrophages and CEBPA, SMAD1 and RUNX1 in U937 cells, were found. Sequencing of the cut sites of two selected sgRNAs validated the functional requirements of some of these binding sites (Fig. 2, Supplementary Material, Fig. S7). Third, at the 3′ end of intron 1, we found binding of STAT1 in LPS-stimulated CD14$^+$ monocytes; and SPI1 in DCs and IFN-γ-treated macrophages. To confirm the importance of SPI1 that recurred in multiple regions and cell types, we targeted the *SPI1* gene with CRISPRi and indeed found reduced FCGR2A levels (1.5-fold reduction, $P = 0.0061$; Supplementary Material, Table S8). As a comparison, depletion of other TFs with a crucial role in monocyte development, such as c-MYC, EGR1 and GATA2 (37), had minor or no effects on FCGR2A expression (Supplementary Material, Table S8). Overall, we found that TFs associated with Subregions 1–2 (in CRISPRi region 3) were enriched in the IL-6-mediated signaling pathway and regulation of immune system processes (Supplementary Material, Tables S3, S5 and S6). The similar enrichment in both subregions for immune-related TFs that are induced by immunostimulatory ligands highlights the importance of regulating FCGR2A expression during inflammation.

FCGR2A regulatory regions harbor genetic variants that affect gene regulation and primary cell protein expression

Next, we wanted to investigate whether there are SNPs that affect FCGR2A expression through modification of its regulatory regions and that are linked to the coding

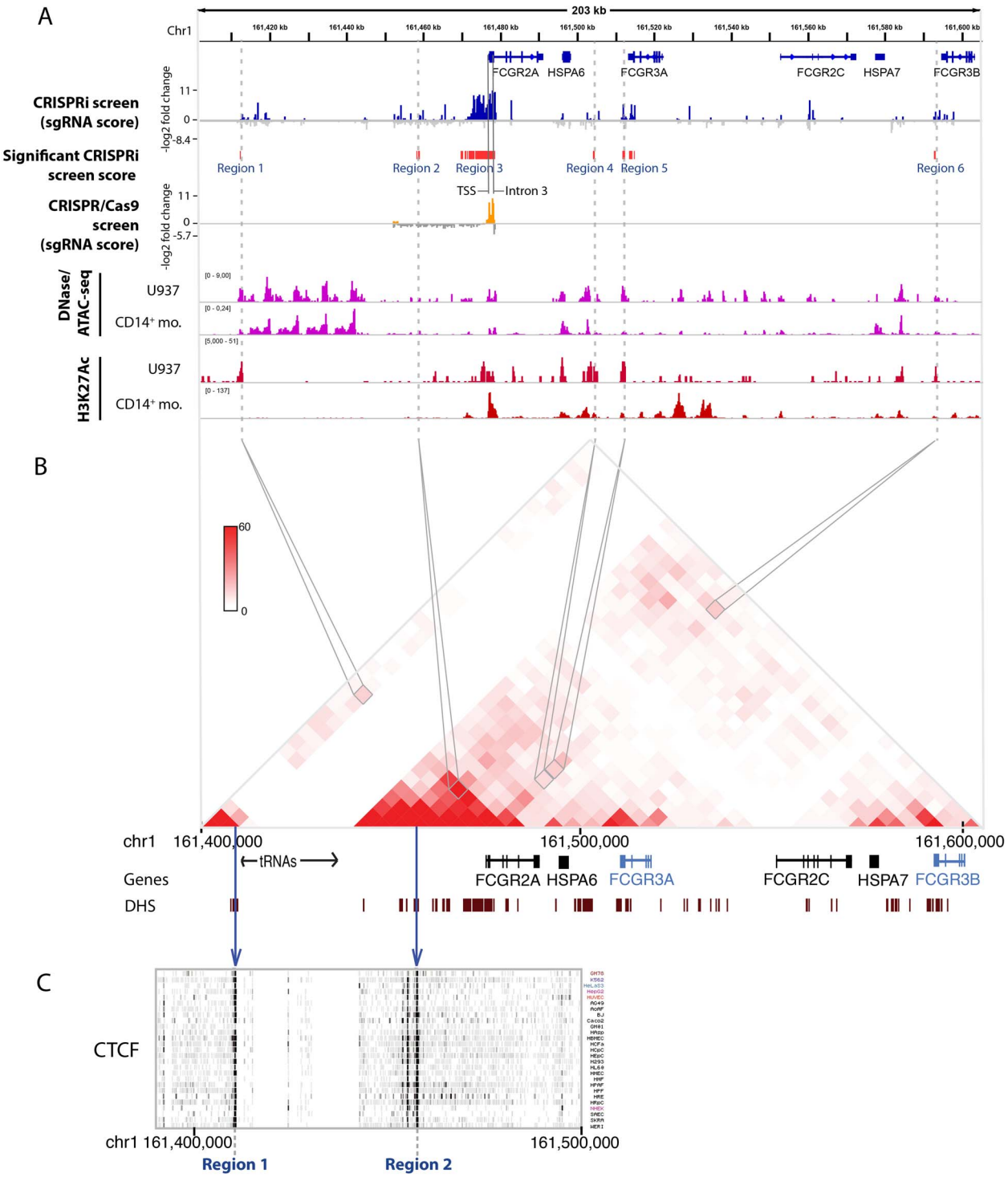

Figure 1. Systematic mapping and characterization of *FCGR2A* regulatory regions. (**A**) CRISPRi screen results of regulatory regions in the FCGR region affecting expression of FCGR2A, depicted as sgRNAs (blue/gray bars). A high CRISPRi score indicates depletion/reduction of FCGR2A expression (−log2 fold change). Red horizontal bars indicate windows with significant effects on FCGR2A expression (FDR < 0.05), grouped into regions 1–6. A selected interval starting 25 kb 5′ of *FCGR2A* and ending in intron 3 was further analyzed with a CRISPR/Cas9 screen (sgRNAs represented by orange/gray bars). Locations of TSS and start of intron 3 are marked by gray lines. For CRISPRi/CRISPR results, images are representative of three separate experiments, and are overlayed with U937 ATAC-seq and H3K27Ac ChIP-Seq data (60,68) and $CD14^+$ monocyte (CD14+ mo.) DNase-Seq and H3K27Ac ChIP-Seq data (ENCODE). (**B**) Hi-C data for the FCGR region depicted in (A), with 5 kb resolution in K562 cells (34). Darker red indicates increased chromosomal interactions. Interactions between FCGR2A distal and proximal regulatory regions are enhanced with gray lines/boxes. DHS = DNase hypersensitive sites; 'tRNAs' represent multiple tRNAs. (**C**) CTCF ChIP-seq data for the genomic region surrounding *FCGR2A*, in 27 different cell types (for abbreviations: see ENCODE). Arrows indicate locations of *FCGR2A* regulatory regions 1 and 2. Darker gray/black bars indicate increased binding of CTCF.

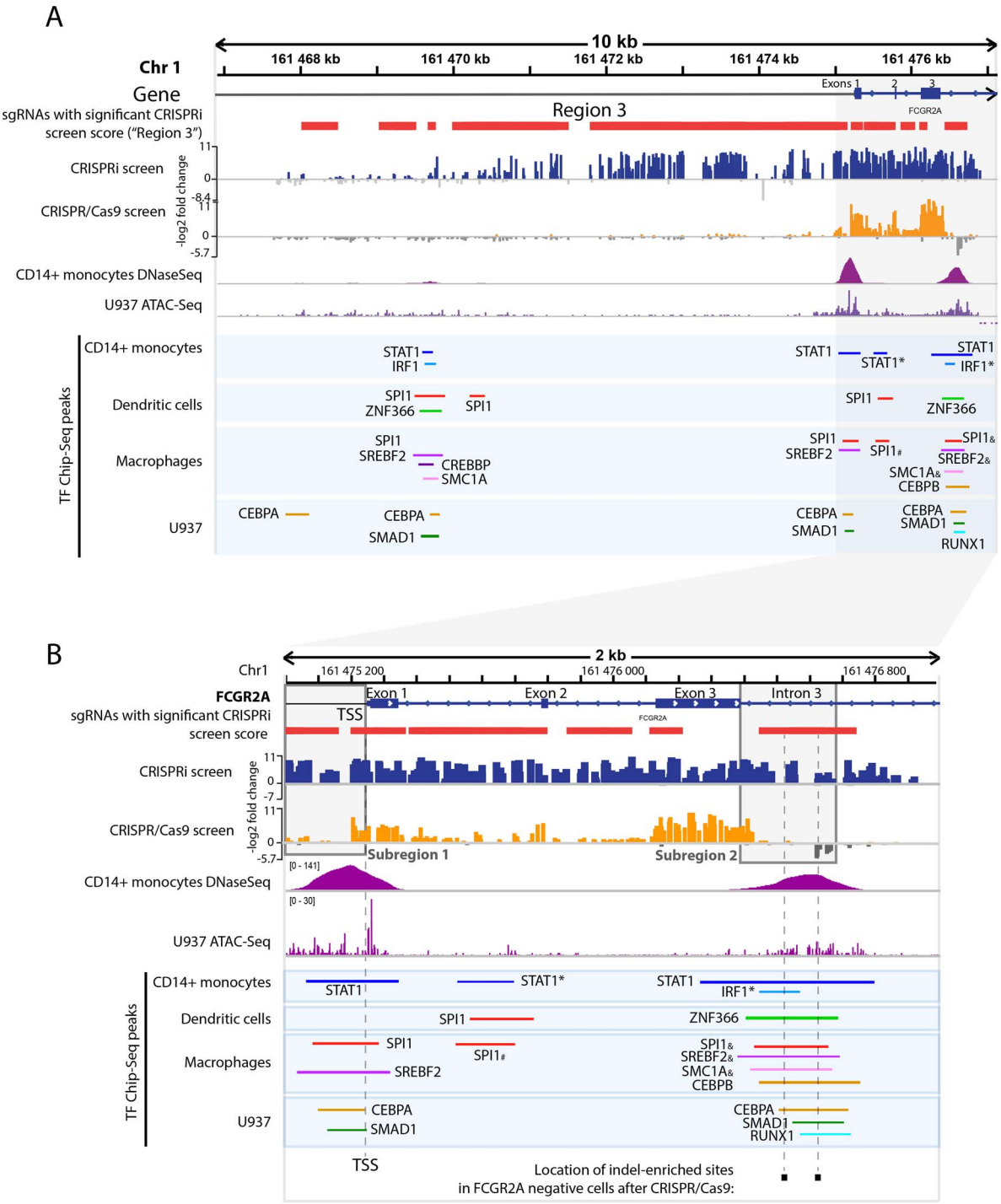

Figure 2. Deep CRISPR/Cas9 and TF analysis of the *FCGR2A* proximal regulatory region. CRISPR/Cas9 screen analysis of the *FCGR2A* putative promoter region, as identified by the CRISPRi screen ('region 3') (**A**), and close-up (**B**). Indicated in red are loci where sgRNAs have a significant effect on FCGR2A expression in the CRISPRi screen; below, each sgRNA of the CRISPRi screen is depicted by a blue bar (20 bp), with −log2 fold change effect on FCGR2A on the y axis. The effects on FCGR2A of the sgRNAs of the CRISPR/Cas9 screen are represented by orange and gray bars (depleting and increasing effects, respectively). Images are representative of three separate experiments. Two non-coding regions with strong effects of sgRNAs on FCGR2A expression are marked by gray boxes (Subregions 1–2) (B). Here, each sgRNA of the CRISPR/Cas9 screen is represented by a bar of 10-bp width to increase resolution of image. Black boxes represent sequenced cut sites of two selected sgRNAs, resulting in reduced FCGR2A expression. The entire region is overlaid with DNaseSeq data of CD14^{+} monocytes (ENCODE), ATAC-seq data of U937 cells (60) and TF ChIP-seq data from the Chip-atlas database of selected myeloid cells. CD14^{+} monocytes were cultured with MCF (10 ng/ml) and showed equal results for STAT1 and IRF1 binding with or without IFN-γ (100 U/ml) for 24 h and with or without treatment with LPS (50 ng/ml) for 3 h (STAT1) or 6 h (IRF1), except for STAT1*/IRF1* (binding in LPS-treated cells only). Macrophages were subject to different treatment regimens (SPI1: IFN-β for 6 h, IFN-γ, TNF-α + PGE2 + Pam3CSK4; SREBF2: TNF-α (10 ng/ml) for 16 h; SMC1A: IFN-γ; CEBPB: oxLDL (50 μg/ml), IFN-γ) and presented equal binding of TF with or without treatment except for SPI1$^{\#}$ (binding with IFN-γ only), SPI1$^{\&}$ (with and without IFN-γ), SMC1A$^{\&}$ (with IFN-γ) and SREBF2$^{\&}$ (with TNF- α).

variant rs1801274, the SNP in *FCGR2A* to which the association with several diseases has been attributed (7,8,12–14). Eight candidate SNPs that were located in the CRISPRi-identified regulatory regions and that were in LD with the missense variant rs1801274 were selected for analysis of allele-specific effects on luciferase expression in 293T-HEK cells (Supplementary Material, Table S9). For two of the SNPs, there was a >2-fold difference in luciferase expression between reference and alternative allele (Alt.), with the alternative allele reducing gene expression for rs142120486 ($P = 3.6 \times 10^{-9}$) and increasing expression for rs10494360 ($P = 0.013$; Fig. 3A–E). The first SNP, rs142120486, is located at the center of a CTCF binding motif in CRISPRi region 2, changing a critical G to C (38) and causing an ∼50% decrease in luciferase reporter expression (Fig. 3A–C; Supplementary Material, Fig. S8). Rs142120486 is rare (minor allele frequency [MAF] 0.026, GnomAD Europe) and in tight LD with the coding variant rs1801274, although with a low r^2 value due to the discrepancies in MAF between the two SNPs (r^2 0.015, D′ 1.0, CEU). The second SNP, rs10494360 (MAF 0.13), is located within a DC SPI1 ChIP-Seq peak in intron 1 of *FCGR2A*, is also in tight LD with rs1801274 (r^2 0.19, D′ 0.94, CEU) and has previously been shown to be the lead SNP with a suggestive association with RA [(19); Fig. 3A, D and E; Supplementary Material, Fig. S8]. Thus, our analysis identified two genetic variants that affect reporter gene expression and that are in tight LD with a coding disease-associated SNP.

To determine whether *FCGR2A* regulatory variants also have an effect on FCGR2A levels on the cell surface of primary myeloid cells, we selected the more common of the two variants identified above (rs10494360) for a protein quantitative trait locus (pQTL) analysis. It was previously shown that rs1801274 is associated with the proportion of FCGR2A/B positive 'inflammatory' monocytes/DCs ($CD123^-CD11C^+CD1C^-CD16^+$) and $CD14^+CD16^{low}$ monocytes, but not B cells (39), using flow cytometry with an antibody that stains both FCGR2A and B. Hence, we selected these cell types for pQTL analysis, from a data set comprising PBMCs and genome-wide genotype data from 1996 individuals. Confirming previous results, rs1801274 was highly associated with the percentage of FCGR2A/B positive inflammatory monocytes/DCs and $CD14^+CD16^{low}$ monocytes, but not B cells ($P = 2.9 \times 10^{-133}$, $P = 3.2 \times 10^{-216}$ and $P = 8.4 \times 10^{-3}$, respectively; Fig. 4A). Equally strong was the association between rs10494360 and FCGR2A/B positive cells, where a homozygous state of rs10494360-A was associated with almost 100% FCGR2A/B positive inflammatory monocytes/DCs and $CD14^+CD16^{low}$ monocytes, but not B cells ($P = 6.5 \times 10^{-241}$, $P = 1.9 \times 10^{-164}$ and $P = 5.3 \times 10^{-10}$, respectively; Fig. 4B). Combining the two SNPs into a diplotype increased the signal of association in inflammatory monocytes/DCs and $CD14^+CD16^{low}$ monocytes ($P = 1.7 \times 10^{-297}$ and $P = 5.1 \times 10^{-299}$; Fig. 4C). Since FCGR2A is not expressed in B cells, whereas FCGR2B is highly expressed in B cells and has a lower expression in myeloid cells, we conclude from these results that the identified variant rs10494360 contributes to variability of FCGR2A expression.

Discussion

FCGR2A plays a central role in regulating and responding to antibody–antigen complexes. To address the major gap in our mechanistic understanding of how this gene is regulated, we characterized *cis* elements and autoimmunity-associated genetic variants that control *FCGR2A* expression. We found one extensive proximal genomic region (region 3) and five distal regions that influence FCGR2A expression. The most proximal regulatory region is comprised of two subregions, with the intronic region likely acting as an enhancer to the TSS-associated subregion or with both regions acting as alternative promoters. The existence of two proximal subregions, and repressive and enhancing effects of the 3′ subregion, suggest a complex regulatory control region for the gene.

Our approach to identify these regions was systematic, combining the strong effects of CRISPRi with the high resolution of CRISPR/Cas9 to generate a functional map of the larger *FCGR2A* regulatory landscape and a detailed analysis of proximal region elements, respectively. CRISPRi is acknowledged for its efficiency in silencing small and large regulatory regions through formation of heterochromatin (23,25,40,41), but can only achieve a limited resolution. Using CRISPR/Cas9, we increased resolution at target sites, while recognizing the limitations of this method; including false negatives due to variation in sgRNA efficacy, and the simultaneous effects of indels on both transcripts and regulatory elements in the 5′ untranslated region and nearby coding regions. In addition to these technical limitations, we may have also missed other modes of regulation, including: (1) gene regulation affected by copy number variations characterizing this region (42,43); (2) regulatory regions found only in primary monocytes under certain conditions and (3) the effects of potentially shared use of the five distal enhancers with other genes (such as other FCGRs, *ATF6* and *DUSP12*) on regulation of *FCGR2A*.

The coding variant rs1801274 in *FCGR2A* has been associated with several autoimmune disorders, with the two alleles associated with the risk of different diseases, e.g. rs1801274-G with SLE and rs1801274-A with Kawasaki's disease (12–14). The rs1801274-G allele exhibits reduced affinity and capacity to phagocytose IgG2-containing ICs, being the leading hypothesis as to how the *FCGR2A* locus is mechanistically implicated in SLE (44). Weaknesses in this existing model include that the difference in affinity to IgG2 is reduced in contexts with high concentrations of IgG2 ICs or in inflammatory milieus with reactive oxygen species (15,45) and that genetic analyses of posterior probabilities for causal variants in disease have pointed in the direction non-coding variants (16,17). Here, we provide evidence

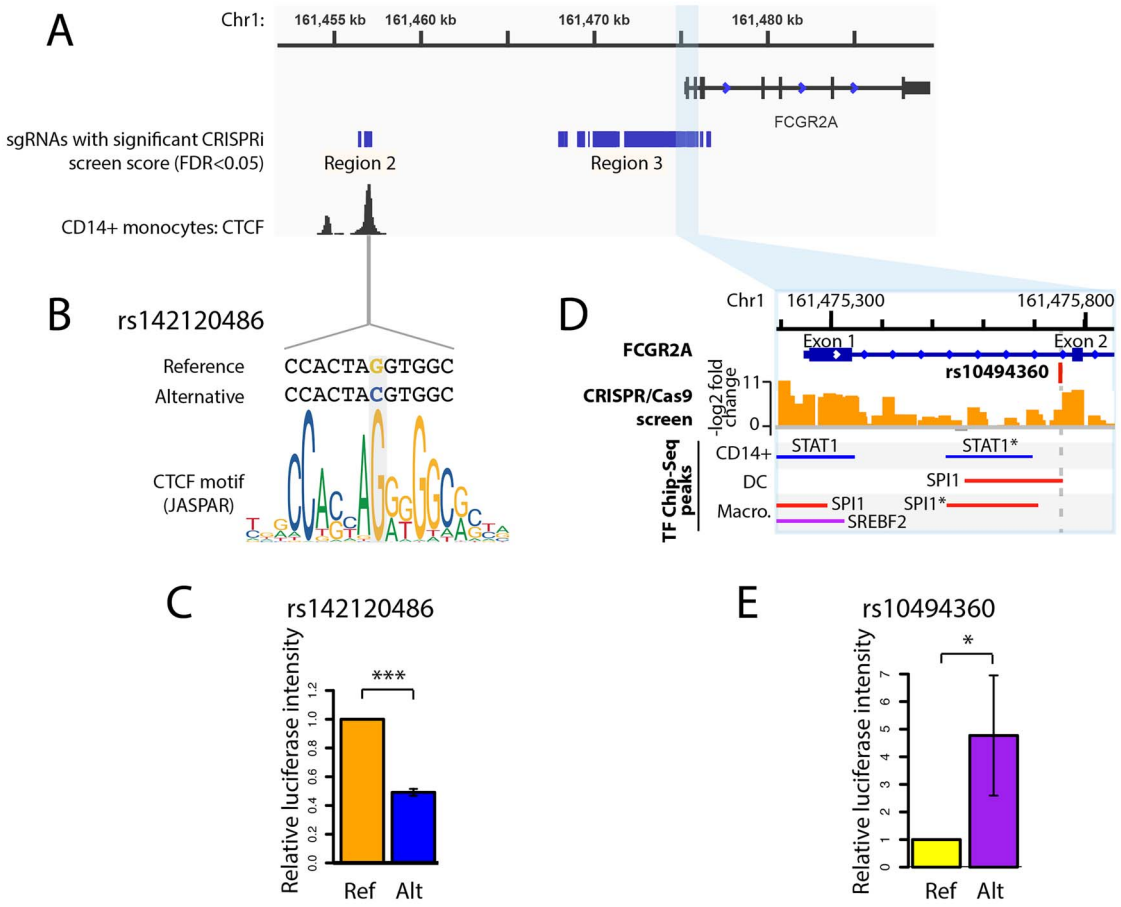

Figure 3. Allele-specific effects on gene expression of genetic variants localized to *FCGR2A* regulatory regions. (**A**, **B**) rs142120486 (G/C) is located in CRISPRi region 2 (chr1:161 456 982), at the center of a CTCF binding motif (ENCODE; JASPAR database). (**C**) Luciferase analysis of allele-specific effects of rs142120486 on gene expression. (A, **D**) Effects of CRISPR/Cas9 screen cutting in the region around the intronic variant rs10494360 (G/A) (at chr1:161475750, 26 bp from exon 2; CRISPRi region 3) on *FCGR2A* expression. Region is overlapped with TF ChIP-Seq peaks of $CD14^+$ monocytes, dendritic cells (DC) and macrophages (macro.) (Chip-atlas). (D) Luciferase analysis of allele-specific effects of rs10494360 on gene expression. Ref = reference allele; Alt = alternative allele. *$P < 0.05$; *** $P < 0.001$.

of functional non-coding SNPs at the FCGR2A locus, consistent with the principles that non-coding SNPs can modify TF-binding motifs and thus affect cell type-specific phenotypes and disease susceptibility (46). In particular, we discovered that the rare variant rs142120486 is located in the center of a CTCF motif in one of the 5′ distal regulatory regions and that the motif-disruptive allele reduced downstream gene expression. This is consistent with findings that CTCF binding to regions interspersed between enhancers and promoters, rather than to TAD boundaries, facilitates enhancer-promoter interactions and thereby transcriptional activation (47). Alternatively, loss of CTCF binding may inhibit recruitment of TFs to this particular site, leading to reduced gene expression. Moreover, the alternative A allele of the intronic SNP rs10494360 significantly increased gene expression and was strongly associated with a high proportion of FCGR2A/B positive myeloid cells.

These SNPs have not been associated with autoimmune disease at a genome-wide level, although rs10494360-A has a suggestive signal of association with RA [$P = 3.2 \times 10^{-7}$; (19)], but they are in LD with the disease-associated coding variant, with the rare alleles linked to rs1801274-A. Subsequently, the effects of these SNPs on FCGR2A expression are tagged to the receptor's affinity for IgG2 and possibly contribute to susceptibility to autoimmune disease. An interesting hypothesis is that differential levels of FCGR2A have distinct impacts on the development of different autoimmune diseases. In this model, in patients carrying rs10494360-A, inflammation would be fueled by high levels of FCGR2A, mediating phagocytosis and cross-presentation of autoantigens (such as citrullinated peptides) to $CD4^+$ T cells in RA and cytotoxicity and phagocytosis in response to anti-endothelial antibodies in Kawasaki's disease (48). In contrast, because the inflammation in SLE is partly driven by deposition of ICs in small vessels, low FCGR2A levels, in combination with lower affinity of FCGR2A for IgG2-based ICs, would result in reduced removal of ICs, thus exacerbating the inflammation and tissue damage induced by the deposited ICs.

Finally, we observed that TFs binding to *FCGR2A* regulatory regions (especially the proximal region) are associated with pathways of acute inflammation and induction by pathogen-associated recognition patterns

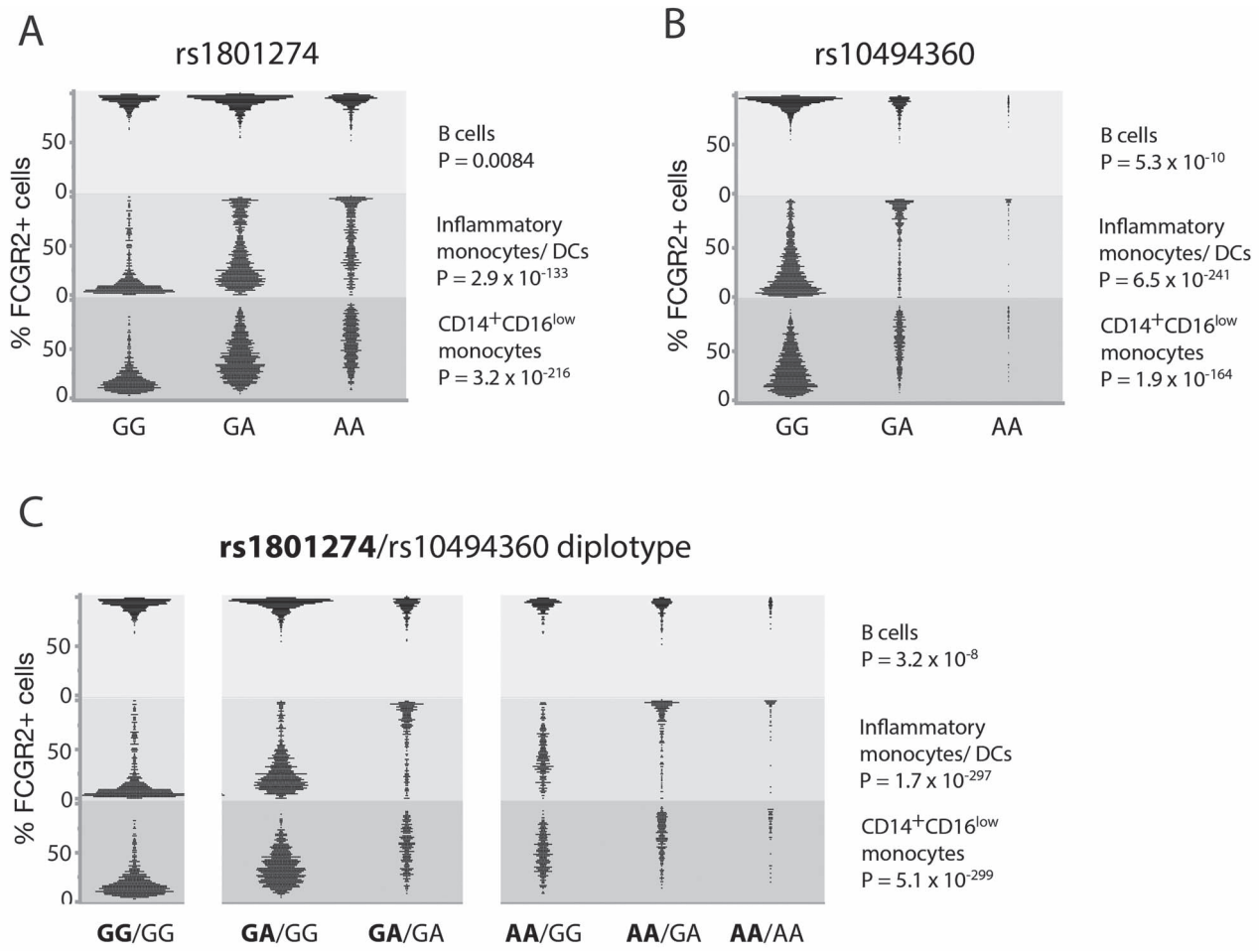

Figure 4. FCGR2A genetic variants rs1801274 and rs10494360 are associated with rate of FCGR2A/B positive myeloid cells. Percentage of FCGR2A/B positive B cells, inflammatory monocytes/dendritic cells (DCs) and $CD14^+$ monocytes categorized by the genotypes of SNPs rs1801274 (**A**) and rs10494360 (**B**) and their combined diplotypes (**C**), as analyzed by flow cytometry of PBMCs from 1996 individuals. Each dot represents one individual. Note, all individuals with genotype rs1801274-G/G also had rs10494360-G/G.

and inflammatory cytokines. Many of these TFs are up- or down-regulated by interferons [e.g. STAT1, IRF1, RUNX1, CEBPA/B, and SREBF2, SPI1, SMAD1, ZNF366, respectively (49)], and engagement of FCG2RA by SLE patient-derived ICs induces IFN-α in plasmacytoid DCs (50), suggesting that *FCGR2A* responds to and regulates the interferon response that may be critical in viral infections and autoimmunity. We also found that SPI1 (PU.1), known for motif enrichment in promoters of genes associated with SLE and RA (51), is a strong regulator of FCGR2A levels, with ChIP-Seq binding signals in 4 of 6 *FCGR2A* regulatory regions. Combined, these findings suggest that the TFs that control *FCGR2A* expression are highly sensitive to environmental signals of inflammation and infection and that regulation of FCGR2A is closely associated with autoimmunity.

Our analysis of the genomic landscape of the *FCGR2A* gene thus identified regulatory regions that are sensitive to environmental cues and proposed regulatory genetic variants. Together, these findings emphasize the importance of gene–environment interactions for immunity and the development of immune-mediated disease.

Materials and Methods

Bulk RNA-sequencing and extraction of single-cell RNA-seq data

To study the direct effect of ICs on *FCGR2A* gene expression, $CD14^+CD16^{low}$ monocytes were sorted from cryopreserved peripheral blood mononuclear cells (PBMCs), prepared using Ficoll-Paque density gradient centrifugation of EDTA-blood samples from 27 healthy participants of the ImmVar project (52–54). Upon thawing, cells were stained with fluorescently labelled antibodies (Supplementary Material, Table S10) in 1 × PBS, 0.5% BSA and 2 mM EDTA (FACS buffer) for 30 min on ice, washed once and sorted for $DAPI^-$ $CD3^-CD19^-CD56^-CD16^-$ $HLA\text{–}DR^+CD14^+$ cells using MoFlo Astrios Sorter (Beckman Coulter, Danvers, MA, USA). $CD14^+$ monocytes were plated on Day 0 at a density of 50 000 cells in 50 μl of standard cell culture medium (RPMI-1640, 10% HIFBS (both Thermo Fisher Scientific, Waltham, MA, USA), 2 mM L-glutamine, 100 units/ml streptomycin, 100 mg/ml penicillin) per well with two wells per individual in non-treated 96-well-plates and kept at 37°C and 5% CO_2, in a humified incubator. At Day 1, latex bead-rabbit IgG ICs (Cat. no. 500 290;

Cayman Chemical, Ann Arbor, MI, USA) were added to one well/individual at a concentration of 1:50. After 4 h, cells were spun down, washed and resuspended in TCL buffer (Qiagen, Hilden, Germany) with 1% β-mercapto-ethanol and frozen until RNA was prepared using the Smart-Seq2 protocol (55). Samples were sequenced with Illumina NovaSeq to an average depth of 30M read pairs of length 50 nt, which were aligned to the GENCODE v.19 transcriptome using STAR v2.6 and quantified with RSEM v1.2.31. The R package DESeq2 was used to find differentially expressed genes between $CD14^+$ sorted cells that were stimulated with ICs and those that were not, controlling for donor. Differences in FCGR2A mRNA levels between IC-treated and non-treated cells were calculated using Wald test.

FCGR2A transcript levels were analyzed in two separate single-cell RNA-seq (scRNA-seq) data sets of our laboratory (32,33). In the first data set, PBMCs from healthy controls and individuals with bacterial sepsis were single-cell RNA sequenced using 3′ v2 profiling chemistry [10X Genomics; (32)]. Transcript levels of *FCGR2A* were compared between cells of healthy and septic individuals in $CD14^+$ monocytes, $CD16^+$ monocytes and $CD1c^+$ DCs, using Wilcoxon rank sum test. For the second data set, cells from intact kidney biopsies from 24 patients with lupus nephritis were sorted into 384-well plates and RNA sequenced using a modified CEL-seq2 protocol (33,56). Differential expression of *FCGR2A* between the myeloid clusters CM0, CM1 and CM4, was analyzed using the framework proposed by McDavid *et al.* (33,57).

Tissue culture

U937 cells were cultured in standard cell medium under conditions as described earlier. 293T-HEK cells were cultured in DMEM (VWR, Radnor, PA, USA) with 10% HIFBS, 2 mM L-glutamine, 100 units/ml streptomycin and 100 mg/ml penicillin and were split at 80% confluence. Only 293T-HEK cells of passage < 10 were used for all experiments. All cell lines were acquired from the Broad Institute stock.

Chromosome conformation capture-on-chip sequencing (4C)

To identify chromosomal regions interacting with the FCGR2A promoter, 4C was performed with a protocol adapted from Rao *et al.* (34). In brief, 2–5 million U937 cells were cross-linked with 1% v/v formaldehyde for 10 min during mixing and reactions were quenched using 0.2M glycine. After washing, cells were lysed for 15 min using 300 ul ice-cold 4C lysis buffer (10 mM Tris–HCl pH 8.0, 10 mM NaCl, 0.2% Igepal CA630) with 50 μl of protease inhibitors (Sigma/Merch, Darmstadt, Germany, P8340). Pelleted nuclei were washed and resuspended in 50 μl of 0.5% sodium dodecyl sulfate (SDS) and incubated at 62°C for 5–10 min and reactions were then quenched using 145 μl of water and 25 μl of 10% Triton X-100 (Sigma, 93 443). Next, chromatin was digested using DpnII and NlaIII restriction enzymes (New England Biolabs (NEB), Ipswich, MA, USA) with the following procedure for each enzyme: restriction enzyme was added together with 10X NEB CutSmart and incubated for 2 h at 37°C with rotation. Reactions were inactivated at 62°C, followed by ligation using the ligation master mix [663 μl of water, 120 μl of 10X T4 DNA ligase buffer (NEB), 100 μl of 10% Triton X-100, 12 μl of 10 mg/ml bovine serum albumin (100X BSA), 5 μl of 400 U/μl T4 DNA ligase (NEB)] with samples at room temperature for 4 h with rotation. Cells were then pelleted at 2500 g for 5 min, and the supernatant discarded, followed by resuspension in 300 μl buffer (10 mM Tris 0.5 M NaCl, 1% SDS) and addition of 50 μl proteinase K with incubation at 55°C for 30 min. The temperature was then increased up to 68°C overnight. Samples were ethanol precipitated and then purified using 1X Agencourt XP beads (Beckman Coulter). To quantify library, quantitative real-time reverse transcriptase PCR (qPCR) was used to amplify using anchor primers 5′ and 3′ of the *FCGR2A* TSS (chr1:161475247; FANTOM5) with Nextera P5 and P7 sequencing adapters (primers: 5′:TCGTCGGCAGCGTCAGATGTGTATAAGAGACAGTTACT GTTCTGCTGGCCGGT, 3′:GTCTCGTGGGCTCGGAGATGTG TATAAGAGACAGTCCATTCTGCACCAAACATTCA). The cycle number for the sample to cross threshold in the qPCR was used to determine the number of PCR cycles for library amplification and hence PCR was run for 23 cycles with 100 ng 4C DNA library and NEBNEXT 2X master mix (NEB). Samples were purified using 1X Agencourt XP beads, resuspended in 50 μl Buffer EB, quantified using Qubit (Thermo Fisher Scientific), quality assessed using tape station and finally sequenced using Illumina MiSeq.

In data analysis, we identified reads derived from ligation of distant chromatin interactions using the Bioconductor Basic4Cseq package. We determined regions that contact the *FCGR2A* promoter (chr1:161 475 029–161 475 562) according to enrichment of reads from NlaIII/DpnII fragments (from 4C BAM files), focusing on fragments within 600 kb (chr1:161 200 000–161 800 000; GEO accession no. GSE180154).

CRISPRi and CRISPR/Cas9 screens: selection of targets for sgRNAs

A CRISPRi screen was designed covering the FCGR2A TAD as identified by 4C in U937 cells and two additional TADs in each direction as identified by published data for K562 cells [Note: the K562 cell line was consistently used for database mining throughout the study as a proxy for myeloid cells, as it is thoroughly studied in comparison with U937 and primary cells; for identification of TADs and chromosomal interactions, THP-1 data at a lower resolution were also used; (34,35,58)], in total ~1.7 Mb (chr1:160 641 952–162 389 706; Supplementary Material, Fig. S3). Within the 5 TADS, sgRNAs were designed to tile regions of open chromatin, for which DNase-seq data were extracted for K562 and Karpas422 cell lines [ENCODE; (59)] and assay for transposase-accessible

chromatin with high-throughput sequencing (ATAC-seq) data were used for U937 and BJAB cell lines [GEO accession no. GSM4055241, GSM4055235; (60)]. Regions of open chromatin were defined as center of peak ±250 bp.

For the region ∼25 kb 5′ of FCGR2A including the putative promoter region, an additional set of sgRNAs was designed and cloned; these sgRNAs were transduced mixed with the original larger set of sgRNAs covering the 1.7 Mb region for the CRISPRi screen, but also used as a separate screen of the putative promoter region, using CRISPR/Cas9. This set of sgRNAs tiled regions within chr1:161 450 383–161 476 919 characterized by histone modifications associated with gene regulation in $CD14^+$ monocytes and K562 cells, as assessed by eyeball of ENCODE H3K4me1 and H3K27Ac ChIP-Seq data (Supplementary Material, Table S7).

For the identification of TFs that affect FCGR2A expression, sgRNAs targeting the TSS of 23 different TFs were included in the pool of sgRNAs for the CRISPRi screen (Supplementary Material, Tables S8 and S11). The TFs were selected based on either published Chip-Seq data (ENCODE) for TFs binding 5′ of or within the FCGR2A gene in K562 cells or $CD14^+$ monocytes, or literature with TFs being implicated in myeloid cell processes. For each TF transcript, the top 2–8 sgRNAs as identified by Horlbeck *et al*. (61) were selected for CRISPRi.

Lastly, as negative controls, 1000 NTsgRNAs with scrambled sequences, randomly selected from those designed by the Weissman lab (62), were cloned as a separate pool of sgRNAs and then transduced together with both the pool of CRISPRi/TF sgRNAs and with the pool of promoter sgRNAs in the CRISPR/Cas9 screen.

CRISPRi and CRISPR/Cas9 screens: sgRNA design and cloning

For the selected regions, we generated a list of all possible sgRNAs flanked by an NGG (protospaces adjacent motif). Since a large part of the FCGR TAD is characterized by a segmental duplication with extensive sequence homology (63), two perfect sgRNA matches were allowed within the target 1.7 Mb region, whereas no perfect matches were allowed in the rest of the genome, with an off-target score limit at 20. sgRNAs were designed to allow GC content between 15% and 85%, with maximum 10 Gs total, whereas sgRNAs with 6 homopolymers of G, C or A or 5 of T and sgRNAs ending with 4 Ts were removed. For cloning into sgOpti vectors, we added a guanine ('G') to the beginning of the sgRNA sequence unless there was already a 'G'.

In total 22 663 targeting sgRNAs were included in the CRISPRi screen (including TF sgRNAs) and 1446 targeting sgRNAs were designed for the promoter CRISPR/Cas9 screen, in addition to the 1000 non-targeting sgRNAs (NTsgRNAs) (Supplementary Material, Table S11). PCR handles were added to the designed sgRNA sequences and the sgRNA library was ordered from CustomArray (Bothell, WA, USA). sgRNAs were cloned into and expressed from sgOpti vectors [modified pLenti-sgRNA (Addgene #71 409)], as previously described (25). Briefly, the pools of sgRNA (CRISPRi screen, CRISPR/Cas9 promoter screen, NTsgRNAs) were PCR amplified using primers adding homology arms for Gibson Assembly (25) and purified using 1X Agencourt XP beads. The sgOpti vectors were digested using BsmBI restriction enzyme (NEB) according to the manufacturer's instructions. sgRNAs and vectors were assembled in a Gibson reaction (NEB) using 70 ng of amplified sgRNAs and 500 ng of vector; assembled vectors were purified with 1X Agencourt XP beads, eluted into 15 μl H_2O and the entire samples were electroporated into Endura competent cells (Lucigen, Middleton, WI, USA). Cells were expanded in liquid culture over night after which the plasmid libraries were prepared using Endotoxin-free Plasmid Maxiprep Kit (Qiagen) and concentrations were measured using Qubit.

dCas9 and Cas9 constructs and expression

For CRISPRi experiments, we used doxycycline (dox)-inducible KRAB-dCas9 constructs with IRES-BFP cassettes and dox-inducible dCas9 U937 and K562 cell lines were established as previously described (25). After lenti-virus cell transduction of constructs, cells were single-cell sorted (fluorescently activated cell sorting, FACS) for BFP positivity using MoFlo Astrios Sorter and a few selected clones were expanded. Subsequent experiments were performed on the expanded single-cell clones with cells resorted in bulk for dox-inducible BFP+ every 3 weeks. For stable Cas9 expression we used the Lenti-Cas9-2A-blast plasmid (addgene #73 310) where the blasticidin resistance gene was replaced by BFP. U937 cells were transduced with the Cas9 construct using lenti-virus and were sorted for BFP+ cells in bulk, using SP6800 Spectral Cell Analyzer (Sony Biotechnology, Bothell, WA, USA).

Lentivirus production

HEK293-T cells were seeded in 6-well-plates at a density of 700 000 cells/well in antibiotic-free cell medium, the day before transfection. Cells were transfected with 500 ng pCMV-R8.74psPAX2 vector, 50 ng VSV-g vector and 500 ng transfer plasmid per well, using TransIT-LT1 (Mirus Bio, Madison, WI, USA) and Optimem (Invitrogen, Waltham, MA, USA). For screen experiments, virus production was performed in 10 cm petri dishes, with the amounts of cells and vectors scaled accordingly. Cell medium was exchanged at 24 h post transfection for cell medium containing 20% HIFBS. Viral supernatants were harvested at 48 and 72 h post transfection and were centrifuged at 1200 g for 10 min to remove cell debris.

Pooled CRISPRi and CRISPR/Cas9 screens

FCGR2A is mainly expressed in myeloid cells, hence the myeloid leukemia cell line U937 was selected for CRISPRi

and CRISPR/Cas9 analysis. In total, three biological replicates were run for each of the CRISPRi and promoter CRISPR/Cas9 screens.

U937 cells carrying either dCas9-KRAB or Cas9 were transduced with pooled gRNA virus at a multiplicity of infection of 0.3 with a coverage of 1000 cells/sgRNA for the CRISPRi screens and ∼11 900 cells/sgRNA for the promoter screen as previously described (64). Twenty-four hours post transduction, cells were split and henceforth cultured in cell medium with 1 μg/ml puromycin, for the selection of successfully transduced cells. Days 2–6 post transduction, cells were split when needed but always kept at a minimum of 1000 and 11 900 cells/gRNA for the CRISPRi and promoter CRISPR/Cas9 screens, respectively. At Day 6, for cells carrying dCas9-KRAB, doxycycline was added to the cell medium at a concentration of 1 μg/ml and cells were cultured for another 5 days before they were harvested. Cas9-expressing cells that had been transduced with the pools of promoter sgRNAs and NTs-gRNAs were harvested at Days 9–14.

Cells were harvested by centrifugation and washed once with 1× PBS. After harvest, 60 million cells/replicate were resuspended in FACS buffer and stained for FCGR2A in two separate tubes of 30 million cells each, treated as two technological replicates of the analysis. For staining, Fab fragments of the anti-FCGR2A antibody IV.3 ('IV.3-Fab'; Stem cell technologies, Vancouver, Canada) were prepared for increased specificity, using Pierce Fab preparation kit (Thermo Scientific) according the manufacturer's instructions and were used at a dilution of 1:10 in the cell-rich samples. Cells were stained on ice for 30 minutes, after which the samples were diluted using FACS buffer, centrifuged and resuspended in FACS buffer for staining with secondary PE-conjugated $F(ab')_2$ anti-Fab (goat anti-mouse; Jackson Immuno Research, Ely, UK) for 30 min on ice. After centrifugation, cells were resuspended at a concentration of 20 million cells/ml in FACS buffer and sorted immediately, with the second technological replicate kept on ice in dark while sorting the first replicate.

Cells were sorted using MoFlo Astrios Sorter into 1× PBS with 50% HIFBS. BFP+ single cells were selected by gating for main cell population according to forward/side scatter, singlets and BFP expression. The BFP+ cells were sorted into two bins at the extremes of PE intensity (lowest and highest, respectively; Supplementary Material, Tables S7 and S11), each comprising 10–12% of all cells (absolute no. of sorted cells/bins varied between 400 000 and 1 300 000), and one bin of non-gated BFP+ cells ('bulk'; no. of cells 150 000–1 000 000). After sorting, cells were spun down, supernatant was removed and cell pellets were stored at −80 until further analysis.

DNA was prepared from cell pellets using DNeasy Blood and Tissue kit (Qiagen) and Proteinase K from NEB with samples eluted in 250 μl H2O and DNA concentrations were measured using Qubit. Samples were divided into 4–8 reactions/sample depending on amount of DNA and were PCR amplified using indexed sgRNA sequencing library primers containing Illumina adaptors (25) and Q5 High Fidelity DNA polymerase (NEB) for 28 cycles. All reactions were verified by running 1 ul/reaction on 2% E-gel EX agarose gels (Thermo Fisher Scientific). PCR reactions were pooled into a total of 3–4 samples, which were purified by running the entire samples on 2% E-gel EX agarose gels followed by gel extraction of the corresponding bands and gel purification using Zymoclean Gel DNA recovery kit (Zymo Research, Irvine, CA, USA). Samples were pooled into one, diluted to a concentration of 0.55 ng/μl and sequenced using Illumina HiSeq2500 and index primers to an average depth of 500 reads/sgRNA. Sequences were aligned to the sgRNA libraries using Bowtie (65), only allowing perfect matches.

CRISPRi score

We identified regions where CRISPRi targeting significantly affected FCGR2A expression as previously described (25). The relative enrichment, or score, of each sgRNA to cell bins sorted based on FCGR2A expression was calculated as the log2 fold-change between the high and low bin for each sgRNA, per replicate. A 'CRISPRi score' was calculated as the mean score of each sgRNA from two separate replicates. To identify significant regions of sgRNAs affecting FCGR2A expression, we compared the CRISPRi scores of 20 consecutive sgRNAs using a sliding window approach, to the scores of NTsgRNAs using *T*-test. Significant regions were defined as those with Benjamini-Hochberg FDR of < 0.05. For the identification of 'significant regions', only sgRNAs with maximum one perfect match in the target region were included. The CRISPRi scores reported in text and figures represent the average of two replicates, normalized to scores of NTsgRNAs (Supplementary Material, Table S1).

For the CRISPRi screen of 23 TFs, 18 out of the 23 TFs had sufficient read counts/sgRNA from all sorted bins. The average log2 scores of the mean of the sgRNAs for each TF from two separate replicates were compared with those of 1000 NTsgRNAs, using Student's *t*-test (Supplementary Material, Table S8).

For the CRISPR/Cas9 promoter screen, the effect of each sgRNA on FCGR2A expression was calculated as the mean score of two replicates.

Screen validation using individual sgRNAs

One or several sgRNAs for each of the six loci identified as significantly affecting FCGR2A expression in the U937 CRISPRi screen were selected for validation based on their physical locations and CRISPRi scores, along with three NTsgRNAs from the screen. sgRNA were cloned into sgOpti vectors and packaged into lentivirus as previously described (66). U937 cells (100 000 cells/well) carrying dCas9 or Cas9 were infected in 96-well-plates using spinoculation at 37°C, 1200 *g* for 30 min with a virus to cell medium ratio of 1:3 and 8 μg/ml polybrene, in a total of 100 μl. Cell medium was changed,

cells split, puromycin selection initiated and doxycycline induction of dCas9 performed as described earlier. dCas9 cells were harvested at Days 5–8 after addition of doxycycline whereas Cas9 cells were harvested at Day 8 after puromycin addition. Cells were stained using IV.3-Fab (1:10) and secondary PE-conjugated $F(ab')_2$ anti-Fab (1:100) as described earlier and FCGR2A expression was analyzed in BFP+ singlet cells using flow cytometry (CytoFLEX, Beckman Coulter). FCGR2A expression levels and percentage of positive cells were analyzed in relation to negative control sgRNAs. All sgRNAs were analyzed in three biological replicates from which the average of median MFI and percentage of positive cells were calculated for each sgRNA, confirming CRISPRi regulatory regions using CRISPRi and in one case CRISPR/Cas9 (Supplementary Material, Table S12; Supplementary Material, Fig. S9). Individual sgRNAs targeting subregions of region 3 from the CRISPR/Cas9 screen were similarly validated using CRISPR/Cas9. When testing individual sgRNAs that increased FCGR2A expression in the screen, we found that some cells increased and others reduced FCGR2A expression, likely due to variability in the length and type of CRISPR-induced genome edits (Supplementary Material, Fig. S7).

Sequence analysis of sgRNA cut sites

The regulatory region of FCGR2A intron 3 was analyzed using next-generation sequencing of induced indels after sgRNAs-targeted Cas9 cutting of this region. U937 cells expressing Cas9 were infected with three selected sgRNAs (Supplementary Material, Table S13) in separate wells. After puromycin selection, cells were FACS sorted for regular, increased and decreased FCGR2A expression, respectively, as compared with NTsgRNA-infected cells, using SP6800 Spectral Cell Analyzer. DNA was prepared using DNeasy Blood and Tissue Kit (Qiagen) and regions of interest were PCR amplified for 35 cycles using specific primers (Supplementary Material, Table S13) and Q5 high fidelity DNA polymerase (NEB). Amplicons were size verified on 2% E-gel EX agarose gels, purified using 1X Agencourt XP beads and concentrations was measured using Qubit. Amplicons were ultra-deep sequenced and mutations were called at Center for Computational and Integrative Biology, Massachusetts General Hospital and indels were analyzed using CRISPResso2 [crispresso2.pinellolab.org; (67)].

Luciferase assay of FCGR2A promoter regions and genetic variation

The two putative promoter regions of FCGR2A as identified by the CRISPR/Cas9 screen (spanning ~200 bp's 5′ of the TSS and ~400 bp's starting at splice donor site of intron 3, respectively) were analyzed for effects on expression using luciferase assay. DNA oligos encompassing 450 bp's, centered on each promoter region were produced with 20 bp Gibson arms at each end, using BioXP (Codex DNA Inc., San Diego, CA, USA; Supplementary Material, Table S9). The 5′ TSS fragment and intron 3 fragment were cloned into firefly luciferase reporter vectors (Promega) without promoter and with a minimal promoter, respectively. Ligation of promoter fragments with vectors was performed using Gibson assembly (NEB) according to the manufacturer's protocol.

Eight candidate SNPs, located in or in the vicinity of *FCGR2A* were analyzed for allele-specific effects on gene expression, also using luciferase assay. The SNPs were selected based on their tight LD with the disease-associated variant rs1801274 ($D' > 0.8$) and that they were located in regulatory regions as identified by the CRISPRi screen (regions 2, 3, 5), overlapping with TF ChIP-Seq peaks and most of them were reported as splice- or expression QTLs (ENCODE, GTex; Supplementary Material, Table S9). DNA oligos encompassing 450 bp's centered on the SNPs (with reference allele) were produced and cloned into firefly luciferase reporter vectors with a minimal promoter as described earlier.

To achieve vectors carrying the opposite allele of each of the eight SNPs, the vectors were mutated using Q5 site-directed mutagenesis according to the instructions of the manufacturer (NEB). Promoter and SNP luciferase plasmids were cloned using Top 10 competent *E. Coli* (Invitrogen) and subsequently prepared using Qiagen Plasmid Plus 96 Miniprep Kit; concentrations were measured using Qubit and sequences were confirmed using Sanger sequencing (Genewiz, South Plainfield, NJ, USA). As myeloid cells are notoriously hard to transfect, 293T-HEK cells were transfected with each vector in quadruplets and co-transfected with Renilla luciferase control vectors (Promega, Madison, WI, USA) for normalization. The ratio between firefly and renilla luciferase was normalized to that of vector without insert. Each vector, or pair of vectors for SNP alleles, were analyzed in a minimum of two biological replicates with the results calculated as average of normalized values of the replicates. SNPs with a ≥2-fold difference in expression levels between the two alleles were considered to have an allele-specific effect on expression, statistically analyzed using Student's *t*-test, as were the differences in expression levels between vectors with promoter inserts versus vectors without inserts.

Intersection of CRISPRi and CRISPR/Cas9 data with epigenetic data and in silico TF analysis

U937 ATAC-seq data were produced in laboratory [see above; (60)] and U937 H3K27Ac ChIP-Seq data were collected from NCBI Gene Expression Omnibus (GEO accession no. GSE111293, (68). $CD14^+$ monocyte DNase-Seq and H3K27Ac ChIP-Seq data were collected from ENCODE.

The complete set of unique TFs shown to bind to any of the six CRISPRi regulatory regions in any cell type through ChIP-Seq analysis (ENCODE) was downloaded and analyzed for gene ontology (GO) enrichment (the Gene Ontology Resource, GOR), as compared with a reference set of 1639 known/likely TFs (http://humantfs.ccbr.utoronto.ca/download.php; Supplementary Material, Tables S4–S6) (69). The six loci were analyzed together and separately.

The CRISPR/Cas9 screen identified gene regulatory subregions spanning from ∼200 bp's 5′ of the *FCGR2A* TSS up to ∼400 bp's into intron 3. TF ChIP-Seq data of primary cell types CD14$^+$ monocytes, macrophages and DCs and of U937 cell line were extracted for this complete region using published data accessible in ChIP-atlas (36). Identified TF's (Fig. 2) were analyzed for GO enrichment as described earlier. TF binding motifs within the CRISPR/Cas9-cut sequenced regions were identified by comparison with consensus TF motifs according to JASPAR (70), MotifMap (71), transcription factor affinity prediction [TRAP; (72)] and for ZNF366 a study by Norskov Sondergaard *et al.* (73).

pQTL analysis of FCGR2A SNPs in selected PBMCs

SNP-dependent regulation of FCGR2 expression on inflammatory monocytes/DCs (CD123$^-$CD11c$^+$CD1c$^-$CD16$^+$), monocytes (CD14$^+$CD16^{low}) and B cells (CD19$^+$CD20$^+$) was assessed as described by Roederer *et al.* (39). Cryopreserved PBMCs from 1996 individuals enrolled in the TwinsUK ($n = 1237$) and VRC ($n = 759$) cohort for which GWAS data were available were treated with FC block and stained with a 28-color B cell/DC panel and analyzed on a FACSymphony as described (74). FCGR2A/B were stained using antibody clone FUN-2, non-selective for FCGR2A/B. Sample processing and data acquisition and pre-processing was performed as described elsewhere (Liechti *et al.*, manuscript in preparation). Data analysis included R-implementation of FlowAI to exclude irregular events (75) and subsequent manual gating using FlowJo 10.7.1 (BD Biosciences, Franklin Lakes, NJ, USA; Supplementary Material, Fig. S10). The association between percentage of FCGR2A/B positive cells and genotypes/diplotypes of rs1801274 and rs10494360 were calculated using one-way analysis of variance.

Data availability

The 4C datasets of this article are available in the NCBI Gene Expression Omnibus (GEO) repository (https://www.ncbi.nlm.nih.gov/geo/), accession no. GSE180154. The CRISPRi and CRISPR/Cas9 datasets supporting the conclusions of this article are included within the article and its additional files. Publicly available datasets were retrieved from the following databases and tools:

Yue Lab, 3D genome browser: http://promoter.bx.psu.edu/hi-c/
ENCODE: http://www.encodeproject.org
ChIP-atlas: http://www.chip-atlas.org
GOR: http://www.geneontology.org
JASPAR: http://jaspar.genereg.org
TRAP: http://trap.molgen.mpg.de/cgi-bin/cite.cgi
MotifMap: http://motifmap.ics.uci.edu
Interferome 2.01: http://interferome.org
GnomAD v2.1.1: https://gnomad.broadinstitute.org/
LDLink: https://ldlink.nci.nih.gov/
GTex: https://gtexportal.org/

Ethical approvals

The blood samples for bulk RNA-seq were collected as part of the Phenogenetic tissue repository under protocol #: 2006-P-002051/8; Brigham and Women's Hospital. The collection of samples for the pQTL analysis was approved by the NIAID (NIH) IRB and London-Westminster NHS Research Ethics Committee; all participants provided informed consent.

Supplementary Material

Supplementary Material is available at *HMG* online.

Acknowledgements

We thank Drs Tim Spector and Massimo Mangino from the Twins UK cohort for the genetic information on the FCRG2A SNPs associated with the PBMC samples analyzed here.

Conflict of Interest statement. N.H. holds equity and consults for Danger Bio and holds equity in BioNTech. J.M.E. and C.P.F. are inventors on a patent application on CRISPR methods filed by the Broad Institute related to this work (16/337846). C.P.F. is now an employee of Bristol Myers Squibb.

Funding

National Human Genome Research Institute (R01HG008-131-01 to N.H.; K99HG009917, R00HG009917 to J.M.E.); The Wallenberg Foundation Scholarship Program (to J.D.); the Intramural Research Program of the VRC; National Institutes of Health (to T.L., and M.R.); and the Harvard Society of Fellows (to J.M.E.).

References

1. Hoiby, N., Doring, G. and Schiotz, P.O. (1986) The role of immune complexes in the pathogenesis of bacterial infections. *Annu. Rev. Microbiol.*, **40**, 29–53.
2. Kalaaji, M., Fenton, K.A., Mortensen, E.S., Olsen, R., Sturfelt, G., Alm, P. and Rekvig, O.P. (2007) Glomerular apoptotic nucleosomes are central target structures for nephritogenic antibodies in human SLE nephritis. *Kidney Int.*, **71**, 664–672.
3. Weiner, G.J. (2007) Monoclonal antibody mechanisms of action in cancer. *Immunol. Res.*, **39**, 271–278.
4. Bournazos, S., Wang, T.T. and Ravetch, J.V. (2016) The role and function of Fcgamma receptors on myeloid cells. *Microbiol. Spectr.*, **4**. doi: 10.1128/microbiolspec.MCHD-0045-2016.
5. Nimmerjahn, F. and Ravetch, J.V. (2008) Fcgamma receptors as regulators of immune responses. *Nat. Rev. Immunol.*, **8**, 34–47.
6. Liu, Y., Gao, X., Masuda, E., Redecha, P.B., Blank, M.C. and Pricop, L. (2006) Regulated expression of FcgammaR in human dendritic cells controls cross-presentation of antigen-antibody complexes. *J. Immunol.*, **177**, 8440–8447.
7. Bougle, A., Max, A., Mongardon, N., Grimaldi, D., Pene, F., Rousseau, C., Chiche, J.D., Bedos, J.P., Vicaut, E. and Mira, J.P. (2012) Protective effects of FCGR2A polymorphism in invasive pneumococcal diseases. *Chest*, **142**, 1474–1481.

8. Beppler, J., Koehler-Santos, P., Pasqualim, G., Matte, U., Alho, C.S., Dias, F.S., Kowalski, T.W., Velasco, I.T., Monteiro, R.C. and Pinheiro da Silva, F. (2016) Fc gamma receptor IIA (CD32A) R131 polymorphism as a marker of genetic susceptibility to sepsis. *Inflammation*, **39**, 518–525.
9. Raaz, D., Herrmann, M., Ekici, A.B., Klinghammer, L., Lausen, B., Voll, R.E., Leusen, J.H., van de Winkel, J.G., Daniel, W.G., Reis, A. *et al.* (2009) FcgammaRIIa genotype is associated with acute coronary syndromes as first manifestation of coronary artery disease. *Atherosclerosis*, **205**, 512–516.
10. Schneider, D.J., McMahon, S.R., Chava, S., Taatjes-Sommer, H.S., Meagher, S., Ehle, G.L. and Brummel-Ziedins, K.E. (2018) FcgammaRIIa: a new cardiovascular risk marker. *J. Am. Coll. Cardiol.*, **72**, 237–238.
11. Beers, S.A., Glennie, M.J. and White, A.L. (2016) Influence of immunoglobulin isotype on therapeutic antibody function. *Blood*, **127**, 1097–1101.
12. Duits, A.J., Bootsma, H., Derksen, R.H., Spronk, P.E., Kater, L., Kallenberg, C.G., Capel, P.J., Westerdaal, N.A., Spierenburg, G.T., Gmelig-Meyling, F.H. *et al.* (1995) Skewed distribution of IgG Fc receptor IIa (CD32) polymorphism is associated with renal disease in systemic lupus erythematosus patients. *Arthritis Rheum.*, **38**, 1832–1836.
13. McGovern, D.P., Gardet, A., Torkvist, L., Goyette, P., Essers, J., Taylor, K.D., Neale, B.M., Ong, R.T., Lagace, C., Li, C. *et al.* (2010) Genome-wide association identifies multiple ulcerative colitis susceptibility loci. *Nat. Genet.*, **42**, 332–337.
14. Khor, C.C., Davila, S., Breunis, W.B., Lee, Y.C., Shimizu, C., Wright, V.J., Yeung, R.S., Tan, D.E., Sim, K.S., Wang, J.J. *et al.* (2011) Genome-wide association study identifies FCGR2A as a susceptibility locus for Kawasaki disease. *Nat. Genet.*, **43**, 1241–1246.
15. Bruhns, P., Iannascoli, B., England, P., Mancardi, D.A., Fernandez, N., Jorieux, S. and Daeron, M. (2009) Specificity and affinity of human Fcgamma receptors and their polymorphic variants for human IgG subclasses. *Blood*, **113**, 3716–3725.
16. Bentham, J., Morris, D.L., Graham, D.S.C., Pinder, C.L., Tombleson, P., Behrens, T.W., Martin, J., Fairfax, B.P., Knight, J.C., Chen, L. *et al.* (2015) Genetic association analyses implicate aberrant regulation of innate and adaptive immunity genes in the pathogenesis of systemic lupus erythematosus. *Nat. Genet.*, **47**, 1457–1464.
17. Wang, Y.F., Zhang, Y., Lin, Z., Zhang, H., Wang, T.Y., Cao, Y., Morris, D.L., Sheng, Y., Yin, X., Zhong, S.L. *et al.* (2021) Identification of 38 novel loci for systemic lupus erythematosus and genetic heterogeneity between ancestral groups. *Nat. Commun.*, **12**, 772.
18. Raychaudhuri, S., Thomson, B.P., Remmers, E.F., Eyre, S., Hinks, A., Guiducci, C., Catanese, J.J., Xie, G., Stahl, E.A., Chen, R. *et al.* (2009) Genetic variants at CD28, PRDM1 and CD2/CD58 are associated with rheumatoid arthritis risk. *Nat. Genet.*, **41**, 1313–1318.
19. Kim, K., Bang, S.Y., Lee, H.S., Cho, S.K., Choi, C.B., Sung, Y.K., Kim, T.H., Jun, J.B., Yoo, D.H., Kang, Y.M. *et al.* (2015) High-density genotyping of immune loci in Koreans and Europeans identifies eight new rheumatoid arthritis risk loci. *Ann. Rheum. Dis.*, **74**, e13.
20. Kleinjan, D.A. and van Heyningen, V. (2005) Long-range control of gene expression: emerging mechanisms and disruption in disease. *Am. J. Hum. Genet.*, **76**, 8–32.
21. van Arensbergen, J., van Steensel, B. and Bussemaker, H.J. (2014) In search of the determinants of enhancer-promoter interaction specificity. *Trends Cell Biol.*, **24**, 695–702.
22. Shlyueva, D., Stampfel, G. and Stark, A. (2014) Transcriptional enhancers: from properties to genome-wide predictions. *Nat. Rev. Genet.*, **15**, 272–286.
23. Qi, L.S., Larson, M.H., Gilbert, L.A., Doudna, J.A., Weissman, J.S., Arkin, A.P. and Lim, W.A. (2013) Repurposing CRISPR as an RNA-guided platform for sequence-specific control of gene expression. *Cell*, **152**, 1173–1183.
24. Gilbert, L.A., Larson, M.H., Morsut, L., Liu, Z., Brar, G.A., Torres, S.E., Stern-Ginossar, N., Brandman, O., Whitehead, E.H., Doudna, J.A. *et al.* (2013) CRISPR-mediated modular RNA-guided regulation of transcription in eukaryotes. *Cell*, **154**, 442–451.
25. Fulco, C.P., Munschauer, M., Anyoha, R., Munson, G., Grossman, S.R., Perez, E.M., Kane, M., Cleary, B., Lander, E.S. and Engreitz, J.M. (2016) Systematic mapping of functional enhancer-promoter connections with CRISPR interference. *Science*, **354**, 769–773.
26. Thakore, P.I., D'Ippolito, A.M., Song, L., Safi, A., Shivakumar, N.K., Kabadi, A.M., Reddy, T.E., Crawford, G.E. and Gersbach, C.A. (2015) Highly specific epigenome editing by CRISPR-Cas9 repressors for silencing of distal regulatory elements. *Nat. Methods*, **12**, 1143–1149.
27. Sanjana, N.E., Wright, J., Zheng, K., Shalem, O., Fontanillas, P., Joung, J., Cheng, C., Regev, A. and Zhang, F. (2016) High-resolution interrogation of functional elements in the noncoding genome. *Science*, **353**, 1545–1549.
28. Canver, M.C., Smith, E.C., Sher, F., Pinello, L., Sanjana, N.E., Shalem, O., Chen, D.D., Schupp, P.G., Vinjamur, D.S., Garcia, S.P. *et al.* (2015) BCL11A enhancer dissection by Cas9-mediated in situ saturating mutagenesis. *Nature*, **527**, 192–197.
29. Hsu, J.Y., Fulco, C.P., Cole, M.A., Canver, M.C., Pellin, D., Sher, F., Farouni, R., Clement, K., Guo, J.A., Biasco, L. *et al.* (2018) CRISPR-SURF: discovering regulatory elements by deconvolution of CRISPR tiling screen data. *Nat. Methods*, **15**, 992–993.
30. Tycko, J., Wainberg, M., Marinov, G.K., Ursu, O., Hess, G.T., Ego, B.K., Aradhana, L., A., Truong, A., Trevino, A.E. *et al.* (2019) Mitigation of off-target toxicity in CRISPR-Cas9 screens for essential non-coding elements. *Nat. Commun.*, **10**, 4063.
31. Vogelpoel, L.T., Baeten, D.L., de Jong, E.C. and den Dunnen, J. (2015) Control of cytokine production by human fc gamma receptors: implications for pathogen defense and autoimmunity. *Front. Immunol.*, **6**, 79.
32. Reyes, M., Filbin, M.R., Bhattacharyya, R.P., Billman, K., Eisenhaure, T., Hung, D.T., Levy, B.D., Baron, R.M., Blainey, P.C., Goldberg, M.B. *et al.* (2020) An immune-cell signature of bacterial sepsis. *Nat. Med.*, **26**, 333–340.
33. Arazi, A., Rao, D.A., Berthier, C.C., Davidson, A., Liu, Y., Hoover, P.J., Chicoine, A., Eisenhaure, T.M., Jonsson, A.H., Li, S. *et al.* (2019) The immune cell landscape in kidneys of patients with lupus nephritis. *Nat. Immunol.*, **20**, 902–914.
34. Rao, S.S., Huntley, M.H., Durand, N.C., Stamenova, E.K., Bochkov, I.D., Robinson, J.T., Sanborn, A.L., Machol, I., Omer, A.D., Lander, E.S. *et al.* (2014) A 3D map of the human genome at kilobase resolution reveals principles of chromatin looping. *Cell*, **159**, 1665–1680.
35. Phanstiel, D.H., Van Bortle, K., Spacek, D., Hess, G.T., Shamim, M.S., Machol, I., Love, M.I., Aiden, E.L., Bassik, M.C. and Snyder, M.P. (2017) Static and dynamic DNA loops form AP-1-bound activation hubs during macrophage development. *Mol. Cell*, **67**, 1037–1048 e1036.
36. Oki, S., Ohta, T., Shioi, G., Hatanaka, H., Ogasawara, O., Okuda, Y., Kawaji, H., Nakaki, R., Sese, J. and Meno, C. (2018) ChIP-atlas: a data-mining suite powered by full integration of public ChIP-seq data. *EMBO Rep.*, **19**, e46255. doi: 10.15252/embr.201846255.
37. Valledor, A.F., Borras, F.E., Cullell-Young, M. and Celada, A. (1998) Transcription factors that regulate monocyte/macrophage differentiation. *J. Leukoc. Biol.*, **63**, 405–417.

38. Kim, T.H., Abdullaev, Z.K., Smith, A.D., Ching, K.A., Loukinov, D.I., Green, R.D., Zhang, M.Q., Lobanenkov, V.V. and Ren, B. (2007) Analysis of the vertebrate insulator protein CTCF-binding sites in the human genome. *Cell*, **128**, 1231–1245.
39. Roederer, M., Quaye, L., Mangino, M., Beddall, M.H., Mahnke, Y., Chattopadhyay, P., Tosi, I., Napolitano, L., Terranova Barberio, M., Menni, C. *et al.* (2015) The genetic architecture of the human immune system: a bioresource for autoimmunity and disease pathogenesis. *Cell*, **161**, 387–403.
40. Gasperini, M., Hill, A.J., McFaline-Figueroa, J.L., Martin, B., Kim, S., Zhang, M.D., Jackson, D., Leith, A., Schreiber, J., Noble, W.S. *et al.* (2019) A genome-wide framework for mapping gene regulation via cellular genetic screens. *Cell*, **176**, 377–390 e319.
41. Fulco, C.P., Nasser, J., Jones, T.R., Munson, G., Bergman, D.T., Subramanian, V., Grossman, S.R., Anyoha, R., Doughty, B.R., Patwardhan, T.A. *et al.* (2019) Activity-by-contact model of enhancer-promoter regulation from thousands of CRISPR perturbations. *Nat. Genet.*, **51**, 1664–1669.
42. Mueller, M., Barros, P., Witherden, A.S., Roberts, A.L., Zhang, Z., Schaschl, H., Yu, C.Y., Hurles, M.E., Schaffner, C., Floto, R.A. *et al.* (2013) Genomic pathology of SLE-associated copy-number variation at the FCGR2C/FCGR3B/FCGR2B locus. *Am. J. Hum. Genet.*, **92**, 28–40.
43. Nagelkerke, S.Q., Tacke, C.E., Breunis, W.B., Geissler, J., Sins, J.W., Appelhof, B., van den Berg, T.K., de Boer, M. and Kuijpers, T.W. (2015) Nonallelic homologous recombination of the FCGR2/3 locus results in copy number variation and novel chimeric FCGR2 genes with aberrant functional expression. *Genes Immun.*, **16**, 422–429.
44. Warmerdam, P.A., van de Winkel, J.G., Vlug, A., Westerdaal, N.A. and Capel, P.J. (1991) A single amino acid in the second Ig-like domain of the human Fc gamma receptor II is critical for human IgG2 binding. *J. Immunol.*, **147**, 1338–1343.
45. Pricop, L. and Salmon, J.E. (2002) Redox regulation of Fcgamma receptor-mediated phagocytosis: implications for host defense and tissue injury. *Antioxid. Redox Signal.*, **4**, 85–95.
46. Bond, G.L., Hu, W., Bond, E.E., Robins, H., Lutzker, S.G., Arva, N.C., Bargonetti, J., Bartel, F., Taubert, H., Wuerl, P. *et al.* (2004) A single nucleotide polymorphism in the MDM2 promoter attenuates the p53 tumor suppressor pathway and accelerates tumor formation in humans. *Cell*, **119**, 591–602.
47. Ren, G., Jin, W., Cui, K., Rodrigez, J., Hu, G., Zhang, Z., Larson, D.R. and Zhao, K. (2017) CTCF-mediated enhancer-promoter interaction is a critical regulator of cell-to-cell variation of gene expression. *Mol. Cell*, **67**, 1049–1058 e1046.
48. Sakurai, Y. (2019) Autoimmune aspects of Kawasaki disease. *J Investig Allergol Clin Immunol*, **29**, 251–261.
49. Rusinova, I., Forster, S., Yu, S., Kannan, A., Masse, M., Cumming, H., Chapman, R. and Hertzog, P.J. (2013) Interferome v2.0: an updated database of annotated interferon-regulated genes. *Nucleic Acids Res.*, **41**, D1040–D1046.
50. Means, T.K., Latz, E., Hayashi, F., Murali, M.R., Golenbock, D.T. and Luster, A.D. (2005) Human lupus autoantibody-DNA complexes activate DCs through cooperation of CD32 and TLR9. *J. Clin. Invest.*, **115**, 407–417.
51. Dozmorov, M.G., Wren, J.D. and Alarcon-Riquelme, M.E. (2014) Epigenomic elements enriched in the promoters of autoimmunity susceptibility genes. *Epigenetics*, **9**, 276–285.
52. Lee, M.N., Ye, C., Villani, A.C., Raj, T., Li, W., Eisenhaure, T.M., Imboywa, S.H., Chipendo, P.I., Ran, F.A., Slowikowski, K. *et al.* (2014) Common genetic variants modulate pathogen-sensing responses in human dendritic cells. *Science*, **343**, 1246980.
53. Raj, T., Rothamel, K., Mostafavi, S., Ye, C., Lee, M.N., Replogle, J.M., Feng, T., Lee, M., Asinovski, N., Frohlich, I. *et al.* (2014) Polarization of the effects of autoimmune and neurodegenerative risk alleles in leukocytes. *Science*, **344**, 519–523.
54. Ye, C.J., Feng, T., Kwon, H.K., Raj, T., Wilson, M.T., Asinovski, N., McCabe, C., Lee, M.H., Frohlich, I., Paik, H.I. *et al.* (2014) Intersection of population variation and autoimmunity genetics in human T cell activation. *Science*, **345**, 1254665.
55. Picelli, S., Faridani, O.R., Bjorklund, A.K., Winberg, G., Sagasser, S. and Sandberg, R. (2014) Full-length RNA-seq from single cells using Smart-seq2. *Nat. Protoc.*, **9**, 171–181.
56. Hashimshony, T., Senderovich, N., Avital, G., Klochendler, A., de Leeuw, Y., Anavy, L., Gennert, D., Li, S., Livak, K.J., Rozenblatt-Rosen, O. *et al.* (2016) CEL-Seq2: sensitive highly-multiplexed single-cell RNA-Seq. *Genome Biol.*, **17**, 77.
57. McDavid, A., Finak, G., Chattopadyay, P.K., Dominguez, M., Lamoreaux, L., Ma, S.S., Roederer, M. and Gottardo, R. (2013) Data exploration, quality control and testing in single-cell qPCR-based gene expression experiments. *Bioinformatics*, **29**, 461–467.
58. Wang, Y., Song, F., Zhang, B., Zhang, L., Xu, J., Kuang, D., Li, D., Choudhary, M.N.K., Li, Y., Hu, M. *et al.* (2018) The 3D genome browser: a web-based browser for visualizing 3D genome organization and long-range chromatin interactions. *Genome Biol.*, **19**, 151.
59. Consortium, E.P. (2012) An integrated encyclopedia of DNA elements in the human genome. *Nature*, **489**, 57–74.
60. Ray, J.P., de Boer, C.G., Fulco, C.P., Lareau, C.A., Kanai, M., Ulirsch, J.C., Tewhey, R., Ludwig, L.S., Reilly, S.K., Bergman, D.T. *et al.* (2020) Prioritizing disease and trait causal variants at the TNFAIP3 locus using functional and genomic features. *Nat. Commun.*, **11**, 1237.
61. Horlbeck, M.A., Gilbert, L.A., Villalta, J.E., Adamson, B., Pak, R.A., Chen, Y., Fields, A.P., Park, C.Y., Corn, J.E., Kampmann, M. *et al.* (2016) Compact and highly active next-generation libraries for CRISPR-mediated gene repression and activation. *elife*, **5**, e19760. doi: 10.7554/eLife.19760.
62. Gilbert, L.A., Horlbeck, M.A., Adamson, B., Villalta, J.E., Chen, Y., Whitehead, E.H., Guimaraes, C., Panning, B., Ploegh, H.L., Bassik, M.C. *et al.* (2014) Genome-scale CRISPR-mediated control of gene repression and activation. *Cell*, **159**, 647–661.
63. Machado, L.R., Hardwick, R.J., Bowdrey, J., Bogle, H., Knowles, T.J., Sironi, M. and Hollox, E.J. (2012) Evolutionary history of copy-number-variable locus for the low-affinity Fcgamma receptor: mutation rate, autoimmune disease, and the legacy of helminth infection. *Am. J. Hum. Genet.*, **90**, 973–985.
64. Wang, T., Birsoy, K., Hughes, N.W., Krupczak, K.M., Post, Y., Wei, J.J., Lander, E.S. and Sabatini, D.M. (2015) Identification and characterization of essential genes in the human genome. *Science*, **350**, 1096–1101.
65. Langmead, B., Trapnell, C., Pop, M. and Salzberg, S.L. (2009) Ultrafast and memory-efficient alignment of short DNA sequences to the human genome. *Genome Biol.*, **10**, R25.
66. Sanjana, N.E., Shalem, O. and Zhang, F. (2014) Improved vectors and genome-wide libraries for CRISPR screening. *Nat. Methods*, **11**, 783–784.
67. Clement, K., Rees, H., Canver, M.C., Gehrke, J.M., Farouni, R., Hsu, J.Y., Cole, M.A., Liu, D.R., Joung, J.K., Bauer, D.E. *et al.* (2019) CRISPResso2 provides accurate and rapid genome editing sequence analysis. *Nat. Biotechnol.*, **37**, 224–226.
68. Blagitko-Dorfs, N., Schlosser, P., Greve, G., Pfeifer, D., Meier, R., Baude, A., Brocks, D., Plass, C. and Lubbert, M. (2019) Combination treatment of acute myeloid leukemia cells with DNMT and HDAC inhibitors: predominant synergistic gene downregulation associated with gene body demethylation. *Leukemia*, **33**, 945–956.
69. Lambert, S.A., Jolma, A., Campitelli, L.F., Das, P.K., Yin, Y., Albu, M., Chen, X., Taipale, J., Hughes, T.R. and Weirauch,

M.T. (2018) The human transcription factors. *Cell*, **175**, 598–599.
70. Fornes, O., Castro-Mondragon, J.A., Khan, A., van der Lee, R., Zhang, X., Richmond, P.A., Modi, B.P., Correard, S., Gheorghe, M., Baranasic, D. *et al.* (2020) JASPAR 2020: update of the open-access database of transcription factor binding profiles. *Nucleic Acids Res.*, **48**, D87–D92.
71. Xie, X., Rigor, P. and Baldi, P. (2009) MotifMap: a human genome-wide map of candidate regulatory motif sites. *Bioinformatics*, **25**, 167–174.
72. Roider, H.G., Kanhere, A., Manke, T. and Vingron, M. (2007) Predicting transcription factor affinities to DNA from a biophysical model. *Bioinformatics*, **23**, 134–141.
73. Sondergaard, J.N., van Heeringen, S.J., Looman, M.W.G., Tang, C., Triantis, V., Louche, P., Janssen-Megens, E.M., Sieuwerts, A.M., Martens, J.W.M., Logie, C. *et al.* (2018) Dendritic cells actively limit Interleukin-10 production under inflammatory conditions via DC-SCRIPT and dual-specificity phosphatase 4. *Front. Immunol.*, **9**, 1420.
74. Liechti, T. and Roederer, M. (2019) OMIP-051 - 28-color flow cytometry panel to characterize B cells and myeloid cells. *Cytometry A*, **95**, 150–155.
75. Monaco, G., Chen, H., Poidinger, M., Chen, J., de Magalhaes, J.P. and Larbi, A. (2016) flowAI: automatic and interactive anomaly discerning tools for flow cytometry data. *Bioinformatics*, **32**, 2473–2480.